

UC Berkeley

UC Berkeley Previously Published Works

Title

Terahertz Spectroscopy of Tetrameric Peptides

Permalink

<https://escholarship.org/uc/item/32s7k734>

Journal

The Journal of Physical Chemistry Letters, 10(10)

ISSN

1948-7185

Authors

Neu, Jens
Stone, Elizabeth A
Spies, Jacob A
[et al.](#)

Publication Date

2019-05-16

DOI

10.1021/acs.jpcllett.9b01091

Peer reviewed



Published in final edited form as:

J Phys Chem Lett. 2019 May 16; 10(10): 2624–2628. doi:10.1021/acs.jpcllett.9b01091.

Terahertz Spectroscopy of Tetrameric Peptides

Jens Neu¹, Elizabeth A. Stone¹, Jacob A. Spies^{1,2}, Golo Storch¹, Ayaka S. Hatano¹,
Brandon Q. Mercado¹, Scott J. Miller^{1,*}, Charles A. Schmuttenmaer^{1,2,*}

¹Department of Chemistry, Yale University, New Haven, Connecticut 06520, United States

²Energy Sciences Institute, Yale University, West Haven, Connecticut 06516, United States

Abstract

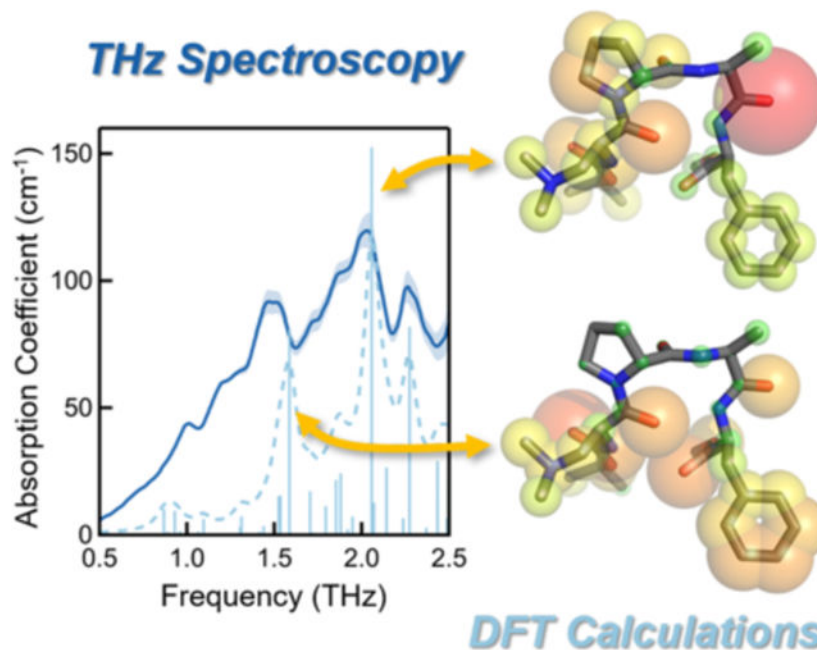
Determining the sequence and structure of peptides is crucial for understanding their structure-property relationships. Among many techniques, structures are typically elucidated using NMR spectroscopy and single crystal X-ray diffraction measurements. In this study, we present terahertz time-domain spectroscopy (THz-TDS) as a complementary, non-destructive technique that is sensitive to both the primary and secondary structures of tetrapeptides. Using only a few milligrams of peptide, THz-TDS spectra have been measured, some of which have been supported by density functional theory (DFT) calculations, to distinguish six tetrameric peptides with similar primary and secondary structures.

Graphical Abstract

*Corresponding Author: scott.miller@yale.edu (S.J.M), charles.schmuttenmaer@yale.edu (C.A.S).

Peptide synthesis and sample preparation procedures; Terahertz spectrometer and data processing details; DFT calculation information (PDF).

Crystallographic data are deposited with the Cambridge Crystallographic Data Centre (CCDC) under the following accession number: 1p (1896374).



Peptides serve a myriad of physiological and biochemical functions, from hormones, antigens, and therapeutics, to artificial sweeteners.¹ These various functions stem, in part, from the structural diversity achieved by noncovalent interactions between and within peptide backbones and side chain residues. While many techniques can be utilized, a combination of NMR spectroscopy and single crystal, X-ray diffraction (XRD) is typically used to elucidate the structure of a sequence-defined peptide. While XRD can clarify primary and secondary solid-state structures, this technique requires suitable crystalline material, which is often non-trivial to obtain. Furthermore, XRD provides a static geometrical structure, which may not capture dynamics occurring in the crystal lattice, which may also provide valuable structural information.

Terahertz time-domain spectroscopy (THz-TDS), which measures IR-active modes in the spectral range of 10–100 cm⁻¹ (1 THz = 33.3 cm⁻¹), is a powerful technique that can provide important structural and dynamical information.^{2–4} In contrast to NMR and XRD, THz spectrometers are less expensive and, once the sample has been prepared, data acquisition takes only seconds. This makes THz-TDS a promising technique for quality control. Since THz radiation is low energy (1 THz photon energy corresponds to $k_B T$ at 48 K), THz-TDS is sensitive to low-frequency inter- and intramolecular vibrational modes in organic molecular crystals. Thus, when cooled to cryogenic temperatures, these modes potentially provide insight into conformational dynamics and structure. Furthermore, the local conformational changes responsible for structure-activity relationships in peptides and proteins often occur on a picosecond timescale (1 ps period corresponds to 1 THz frequency), making THz-TDS ideally suited for studying these motions.^{5–6} Thus, in combination with XRD, THz-TDS provides insight into the dynamic structure of peptides, and in turn, might enable a better understanding of their function.

Despite their versatile functions and biological activity, oligopeptides consisting of more than two different amino acid residues have not been thoroughly studied with TH007A-TDS.^{7–9} The peptides studied herein have been employed as catalysts for the enantioselective bromination of several pharmaceutically relevant compounds.^{10–14} Structurally, the primary sequence contains the Boc-protected catalytically active residue, Dmaa (*i*), followed by either L- or D-proline (*i* + 1) and an α,α -disubstituted amino acid (*i* + 2), which tends to stabilize canonical β -turn secondary structures (Figure 1).^{15–17} In pursuit of elucidating their structures, crystallographic analysis, NMR studies, and DFT calculations of Dmaa-containing peptides revealed a range of conformational states and, in some cases, the same sequence displayed multiple conformers either as symmetry-independent molecules in the same unit cell or as polymorphs.¹⁸ Furthermore, it has been shown that the specific β -turn type of the peptide catalyst largely influences the selectivity achieved in the bromination of arylquinazolinones and diarylmethylamido bis(phenols).^{13–14, 18–20} Due to the large library of solid-state structural information available for this class of peptides, we considered these compounds to be an ideal starting point for THz-TDS studies.

The THz-TDS absorption spectra of the six recrystallized peptides at 65 K are shown in Figure 2. Multiple spectra of each sample were obtained to ensure reproducibility (see Supporting Information). The spectra of these peptides were obtained using only a few milligrams of recrystallized material mixed with Teflon, which is THz transparent.³ Additionally, the spectra of **3** and **5** were measured using as-synthesized material without additional recrystallization. The as-synthesized and recrystallized samples of the same material exhibited no differences in observed resonances (see Figure S2). The ability to obtain high quality THz-TDS spectra without the additional step of recrystallization makes this technique particularly valuable for expeditious structural identification and quality control.

After conducting the THz measurements, the peptide/Teflon pellets were ground into powder, dissolved in acetone via ultrasonication, centrifuged, and recovered in nearly quantitative yields without damaging the structural integrity or purity of the samples, as confirmed by NMR spectroscopy and liquid chromatography-mass spectrometry (Figure S1). Additionally, solid-state density functional theory (DFT) calculations were performed for **4**, **5**, and **6**, which contain two peptides per unit cell. The experimentally obtained crystal structures were used as the starting points for these calculations. This was particularly important, as polymorphism is common for this class of peptides.¹⁸ Indeed, a new polymorphic crystal structure (**1p**) of peptide 1 was identified upon nearly identical recrystallization conditions (Figure 1). A full description of the peptide synthesis, recrystallization conditions, sample preparation, measurement procedures, and DFT calculation details can be found in the Supporting Information.

The first pair of peptides, **1** and **2**, differ solely by the residue at the *i* + 3 position (Phe vs. Leu), yet their THz-TDS signatures are distinct. The spectrum of **1** shows four broad resonances located at 0.78, 1.24, 1.50, and 2.03 THz (Figure 2, black). In contrast, **2** shows a resonance at 0.65 and 2.05 THz, with a number of overlapping resonances between 1.00 – 1.75 THz which makes a rigorous assignment of the individual modes challenging (Figure 2, grey). The most pronounced differences, however, are the strong resonance at 1.83 THz and

a weaker resonance at 1.03 THz, which are both unique to **2**. While these peptides show distinct spectra, they exhibit similar features as well, stemming from their shared secondary structure. For example, the lowest energy resonance shifts from 0.78 to 0.72 THz and the highest shifts from 2.03 to 2.08 THz when Phe is replaced with Leu (Figure 2, black and grey, respectively).

While **1** and **2** vary by a single residue, **3** and **4** differ only in the stereochemistry of the Pro residue. This causes **3** and **4** to favor different β -turn types (Figure 1), which affects their catalytic selectivity.¹⁸ Determining the stereochemistry of the Pro residue to identify these peptides via NMR spectroscopy is quite challenging; however, **3** and **4** exhibit distinct THz signatures (Figure 2, red and orange, respectively). The frequency difference in the resonances, as well as the different number of resonances, are sufficient to distinguish **3** and **4**.

The strong broadening in the spectral characteristics of **4** can be better understood by evaluating the DFT simulated spectrum of this peptide (Figure 3). The calculated spectrum of **4** shows many overlapping resonances, which likely result in the broadening observed in the experimental spectrum. This suggests that the observed line broadening is not caused merely by crystal quality. The agreement between the experiment and DFT spectra is good for peptide **4**, except for the computed resonance at 2.00 THz, which is strongly overestimated due to the numerical method used (Berryphase approach).²¹ Nonetheless, although the sequences of **3** and **4** only differ in the stereochemistry of the Pro residue, the THz spectra are clearly different, demonstrating the sensitivity of THz-TDS to the secondary structure of a peptide.

THz-TDS distinguishes peptide structures **5** and **6**, which have only a slight alteration in primary structure (Acpc vs. Ala, respectively) as seen in Figure 2, blue and purple, respectively. The similar primary and secondary structures of these peptides yielded nearly identical geometric parameters in their crystal structures, as the symmetry groups are the same and the unit cell vectors are within 1% (Figure 1). Therefore, clear crystallographic identification of these peptides requires sufficient single crystals to be measured *via* low-temperature, high-resolution XRD. In comparison, the THz spectrum of **5** can be collected without recrystallization (see Figure S2).

The THz spectra of **5** and **6** show several similarities, once again validating the sensitivity of THz-TDS to their corresponding secondary structures.^{3, 22} However, the spectra also show clear differences, which can be attributed to the variation in primary structure.²³ A clear distinction is observed at 1.98 THz, where **5** has a local minimum and **6** displays a peak. Additionally, the resonances at 1.45 and 2.25 THz for peptide **6** are not observed in **5**. These differences cannot be explained by intuitive arguments, but insight into their origin can be gained using DFT calculations and subsequent mode analysis.

The agreement between the calculated and experimental spectra is comparable to previous work on THz-TDS of organic molecular crystals.^{2, 22–26} The discrepancies may lie in the fundamental difference between solid-state DFT assumptions (perfect, periodic crystal) and experimental reality (polycrystalline powder). Furthermore, the single crystals of the

peptides studied exhibit a distortion in the lattice that is also known to reduce agreement between DFT and experimental characterization.²⁷ The imperfections and finite size of the crystals can cause the lines to broaden and split. The strength and influence of this effect depends on the localization of the mode; hence it exhibits different strengths for different modes. However, the main resonances were reproduced, including the experimentally detected difference between the spectra of **5** and **6**.

From the DFT calculations, eigenvector heatmaps for the two strongest excitations in **5** and **6** were constructed (Figure 4). The heatmap shows the relative displacement of an atom at the indicated resonance frequency, meaning the larger the sphere surrounding an atom, the more it moves when the peptide is excited at this frequency. The lower energy mode of **5** and **6** at approximately 1.6 THz is plotted in panels (a) and (b), respectively, of Figure 4. Both peptides show minimal displacements at the $i + 1$ and $i + 2$ residues, which compose the loop region of the β -turn, with the majority of displacement located at the flexible terminal residues (N -terminal protecting group, i , and $i + 3$ residues). These regions of large displacement are similar in **5** and **6**, which explains why the resonance frequency, strength, and calculated mode character are nearly identical. At the higher frequency, 2.16 THz for **5** and 2.05 THz for **6** (Figure 4 (c) and (d), respectively), the displacement is distributed more evenly over all atoms in each peptide. The stronger contribution of the loop region atoms to the movement explains why this resonance is significantly more sensitive to the change in primary structure which is also localized in the loop region.

In summary, we have shown that THz-TDS is a viable method for distinguishing peptides with similar primary and secondary structures. This non-destructive technique, which does not require single-crystalline samples, provides unique spectral signatures for each peptide, facilitating identification. DFT calculations were used to calculate the dynamic motions of several peptides and visualize the corresponding displacements at strong resonances. Showcasing the sensitivity of THz-TDS towards primary and secondary structures of catalytically active tetrapeptides is an important step towards developing a better understanding of the conformational dynamics that underlie structure-activity relationships in peptides, and potentially proteins.

Supplementary Material

Refer to Web version on PubMed Central for supplementary material.

ACKNOWLEDGMENT

J.N. and C.A.S acknowledge support from the National Science Foundation (CHE-1465085). E.A.S., G. S., and S.J.M acknowledge support from National Institute of General Medical sciences of the NIH (GM-068649 and GM-096403). E.A.S acknowledges the support of the National Science Foundation Graduate Research Fellowship (DGE-112249) and the NIH Molecular Biophysics Predoctoral Training Grant (T32 GM008283). J.A.S. and C.A.S. also acknowledge support from the U.S. Department of Energy, Chemical Sciences, Geosciences, and Biosciences Division, Office of Basic Energy Sciences, Office of Science (DEFG02-07ER15909) and from a generous donation from the TomKat Foundation. G.S. is very grateful for support from the Deutsche Forschungsgemeinschaft (DFG) for a postdoctoral fellowship (STO 1175/1-1). A.S.H. acknowledges support from the Nakatani Foundation (Japan).

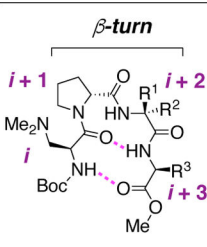
Funding Sources

No competing financial interests have been declared.

REFERENCES

- (1). Sewald N; Jakubke H-D, Peptides: Chemistry and Biology. 2nd ed; Wiley: Weinheim, 2009.
- (2). Williams MRC; Aschaffenburg DJ; Ofori-Okai BK; Schmuttenmaer CA Intermolecular Vibrations in Hydrophobic Amino Acid Crystals: Experiments and Calculations. *J. Phys. Chem. B* 2013, 117, 10444–10461. [PubMed: 23931283]
- (3). Neu J; Nemes CT; Regan KP; Williams MRC; Schmuttenmaer CA Exploring the Solid State Phase Transition in DL-Norvaline with Terahertz Spectroscopy. *Phys. Chem. Chem. Phys* 2018, 20, 276–283.
- (4). Ruggiero MT; Zhang W; Bond AD; Mittleman DM; Zeitler JA Uncovering the Connection Between Low-Frequency Dynamics and Phase Transformation Phenomena in Molecular Solids. *Phys. Rev. Lett* 2018,120, 196002. [PubMed: 29799217]
- (5). Guo J; Zhou H-X Protein Allostery and Conformational Dynamics. *Chem. Rev* 2016,116, 6503–6515. [PubMed: 26876046]
- (6). Woutersen S; Mu Y; Stock G; Hamm P Subpicosecond Conformational Dynamics of Small Peptides Probed by Two-Dimensional Vibrational Spectroscopy. *Proc. Natl. Acad. Sci. U.S.A* 2001,98, 11254–11258. [PubMed: 11553784]
- (7). Xie L; Yao Y; Ying Y The Application of Terahertz Spectroscopy to Protein Detection: A Review. *Appl. Spectrosc. Rev* 2014,49, 448–461.
- (8). Falconer RJ; Markelz AG Terahertz Spectroscopic Analysis of Peptides and Proteins. *J. Infrared Millim. Terahertz Waves* 2012, 33, 973–988.
- (9). Ding T; Middelberg APJ; Huber T; Falconer RJ FarInfrared Spectroscopy Analysis of Linear and Cyclic Peptides, and Lysozyme. *Vib. Spectrosc* 2012, 61, 144–150.
- (10). Gustafson JL; Lim D; Miller SJ Dynamic Kinetic Resolution of Biaryl Atropisomers via Peptide-Catalyzed Asymmetric Bromination. *Science* 2010, 328, 1251–1255. [PubMed: 20522769]
- (11). Barrett KT; Miller SJ Enantioselective Synthesis of Atropisomeric Benzamides through Peptide-Catalyzed Bromination. *J. Am. Chem. Soc* 2013, 135, 2963–2966. [PubMed: 23410090]
- (12). Diener ME; Metrano AJ; Kusano S; Miller SJ Enantioselective Synthesis of 3-Arylquinazolin-4(3H)-ones via Peptide-Catalyzed Atroposelective Bromination. *J. Am. Chem. Soc* 2015, 137, 12369–12377. [PubMed: 26343278]
- (13). Hurtley AE; Stone EA; Metrano AJ; Miller SJ Desymmetrization of Diarylmethylamido Bis(phenols) through Peptide-Catalyzed Bromination: Enantiodivergence as a Consequence of a 2 amu Alteration at an Achiral Residue within the Catalyst. *J. Org. Chem* 2017, 82, 11326–11336. [PubMed: 29020446]
- (14). Metrano AJ; Miller SJ Peptide-Based Catalysts Reach the Outer Sphere through Remote Desymmetrization and Atroposelectivity. *Acc. Chem. Res* 2019, 52, 199–215. [PubMed: 30525436]
- (15). Haque TS; Little JC; Gellman SH Stereochemical Requirements for β -Hairpin Formation: Model Studies with Four-Residue Peptides and Depsipeptides. *J. Am. Chem. Soc* 1996,118, 6975–6985.
- (16). Sibanda BL; Thornton JM β -Hairpin Families in Globular Proteins. *Nature* 1985, 316, 170–174. [PubMed: 4010788]
- (17). Toniolo C; Crisma M; Formaggio F; Peggion C Control of Peptide Conformation by the Thorpe-Ingold Effect ($C\alpha$ -tetrasubstitution). *J. Pept. Sci* 2001, 60, 396–419.
- (18). Metrano AJ; Abascal NC; Mercado BQ; Paulson EK; Hurtley AE; Miller SJ Diversity of Secondary Structure in Catalytic Peptides with β -Turn-Biased Sequences. *J. Am. Chem. Soc* 2017, 139, 492–516. [PubMed: 28029251]
- (19). Crawford JM; Stone EA; Metrano AJ; Miller SJ; Sigman MS Parameterization and Analysis of Peptide-Based Catalysts for the Atroposelective Bromination of 3-Arylquinazolin-4(3H)-ones. *J. Am. Chem. Soc* 2018, 140, 868–871. [PubMed: 29300461]
- (20). Yan XC; Metrano AJ; Robertson MJ; Abascal NC; Tirado-Rives J; Miller SJ; Jorgensen WL Molecular Dynamics Simulations of a Conformationally Mobile Peptide-Based Catalyst for Atroposelective Bromination. *ACS Catal.* 2018, 8, 9968–9979. [PubMed: 30687577]

- (21). King-Smith RD; Vanderbilt D Theory of Polarization of Crystalline Solids. *Phys. Rev. B* 1993, 47, 1651–1654.
- (22). Ruggiero MT; Axel Zeitler J; Korter TM Concomitant Polymorphism and the Martensitic-Like Transformation of an Organic Crystal. *Phys. Chem. Chem. Phys* 2017, 19, 28502–28506. [PubMed: 29043323]
- (23). Neu J; Nikonow H; Schmittenmaer CA Terahertz Spectroscopy and Density Functional Theory Calculations of DL-Norleucine and DL-Methionine. *J. Phys. Chem. A* 2018, 122, 5978–5982. [PubMed: 29894636]
- (24). Nickel DV; Ruggiero MT; Korter TM; Mittleman DM Terahertz Disorder-Localized Rotational Modes and Lattice Vibrational Modes in the Orientationally-Disordered and Ordered Phases of Camphor. *Phys. Chem. Chem. Phys* 2015, 17, 6734–6740. [PubMed: 25461482]
- (25). Witko EM; Korter TM Investigation of the Low-Frequency Vibrations of Crystalline Tartaric Acid Using Terahertz Spectroscopy and Solid-State Density Functional Theory. *J. Phys. Chem. A* 2011, 115, 10052–10058. [PubMed: 21846134]
- (26). King MD; Buchanan WD; Korter TM Understanding the Terahertz Spectra of Crystalline Pharmaceuticals: Terahertz Spectroscopy and Solid-State Density Functional Theory Study of (S)-(+)-Ibuprofen and (R)-Ibuprofen. *J. Pharm. Sci* 2011, 100, 1116–1129. [PubMed: 20815081]
- (27). Ruggiero MT; Sibik J; Orlando R; Zeitler JA; Korter TM Measuring the Elasticity of Poly-L-Proline Helices with Terahertz Spectroscopy. *Angew. Chem. Int. Ed* 2016, 55, 6877–6888.




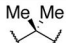
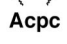

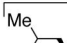
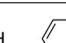
Label	Sequence	a [Å]	b [Å]	c [Å]	α [°]	β [°]	γ [°]	Turn-Type	<i>i</i> + 2	<i>i</i> + 3
1	Boc-Dmaa-D-Pro-Aib-Phe-OMe	9.75	10.83	29.44	90.00	90.00	90.00	II' hairpin		
2	Boc-Dmaa-D-Pro-Aib-Leu-OMe	9.53	10.97	28.98	90.00	90.00	90.00	II' hairpin		
3	Boc-Dmaa-D-Pro-Acpc-Leu-OMe	11.91	15.62	16.46	86.53	89.53	88.98	I' pre-helical		
4	Boc-Dmaa-Pro-Acpc-Leu-OMe	9.93	14.27	11.07	90.00	98.88	90.00	II hairpin		
5	Boc-Dmaa-D-Pro-Acpc-Phe-OMe	10.60	8.89	15.96	90.00	97.12	90.00	II' hairpin		
6	Boc-Dmaa-D-Pro-Ala-Phe-OMe	10.66	8.81	15.86	90.00	97.11	90.00	II' hairpin		

Figure 1.

Solid state structure of β -turn containing peptides (left) with intramolecular hydrogen bonds denoted in pink. The unit cell parameters of the crystalline peptides studied, in addition to the β -turn type, are tabulated in the center.¹⁸ The structures of the *i* + 2 and *i* + 3 residues are also included (right). Abbreviations: Boc, *tert*-butoxycarbonyl; Dmaa, β -dimethylaminoalanine; Acpc, 1-aminocyclopropyl-1-carboxamide; Aib, α -aminoisobutyramide.

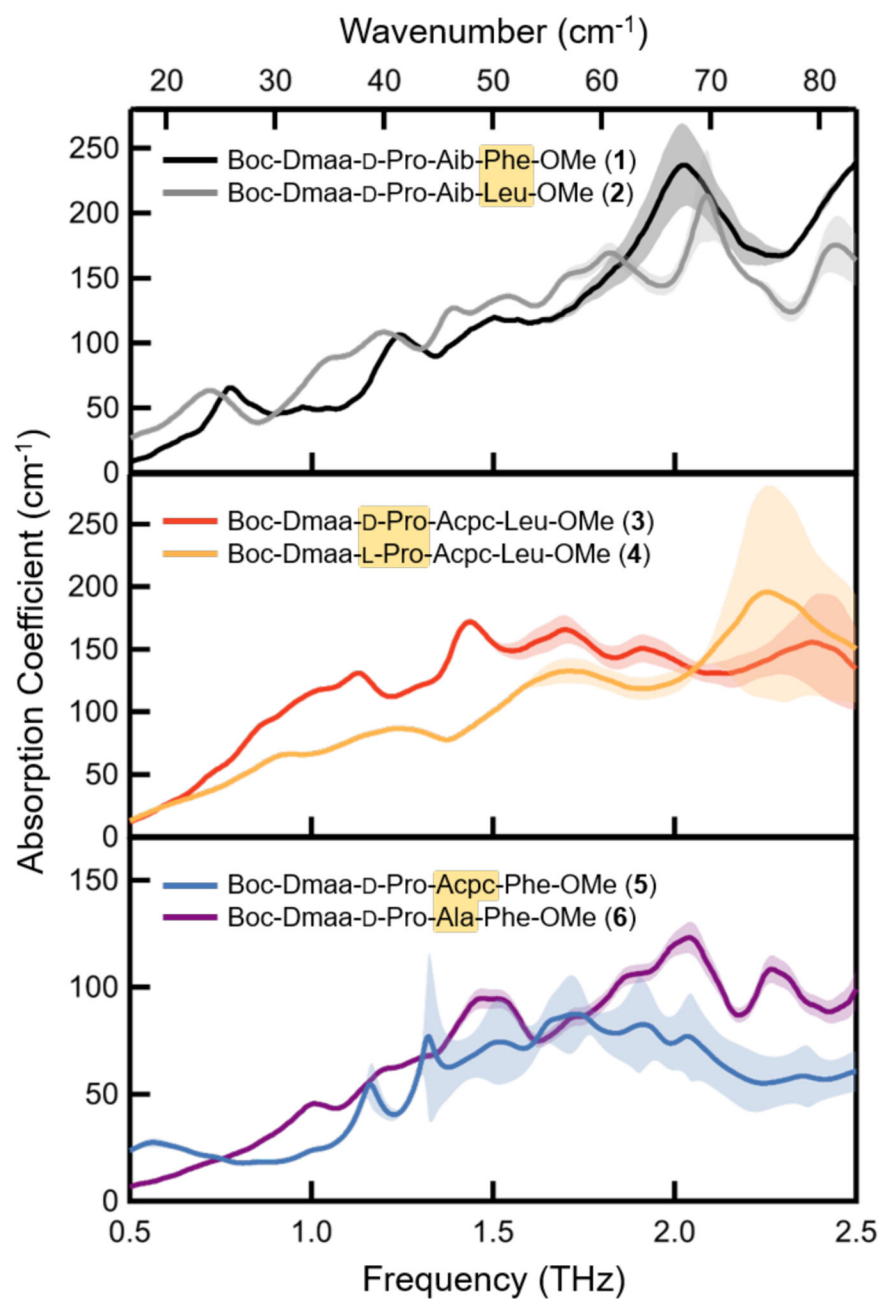


Figure 2. Experimental THz absorption spectra of each peptide at 65 K. The spectral data are paired by single residue structural changes (highlighted in each legend). Standard deviations are shown by shading around each spectrum.

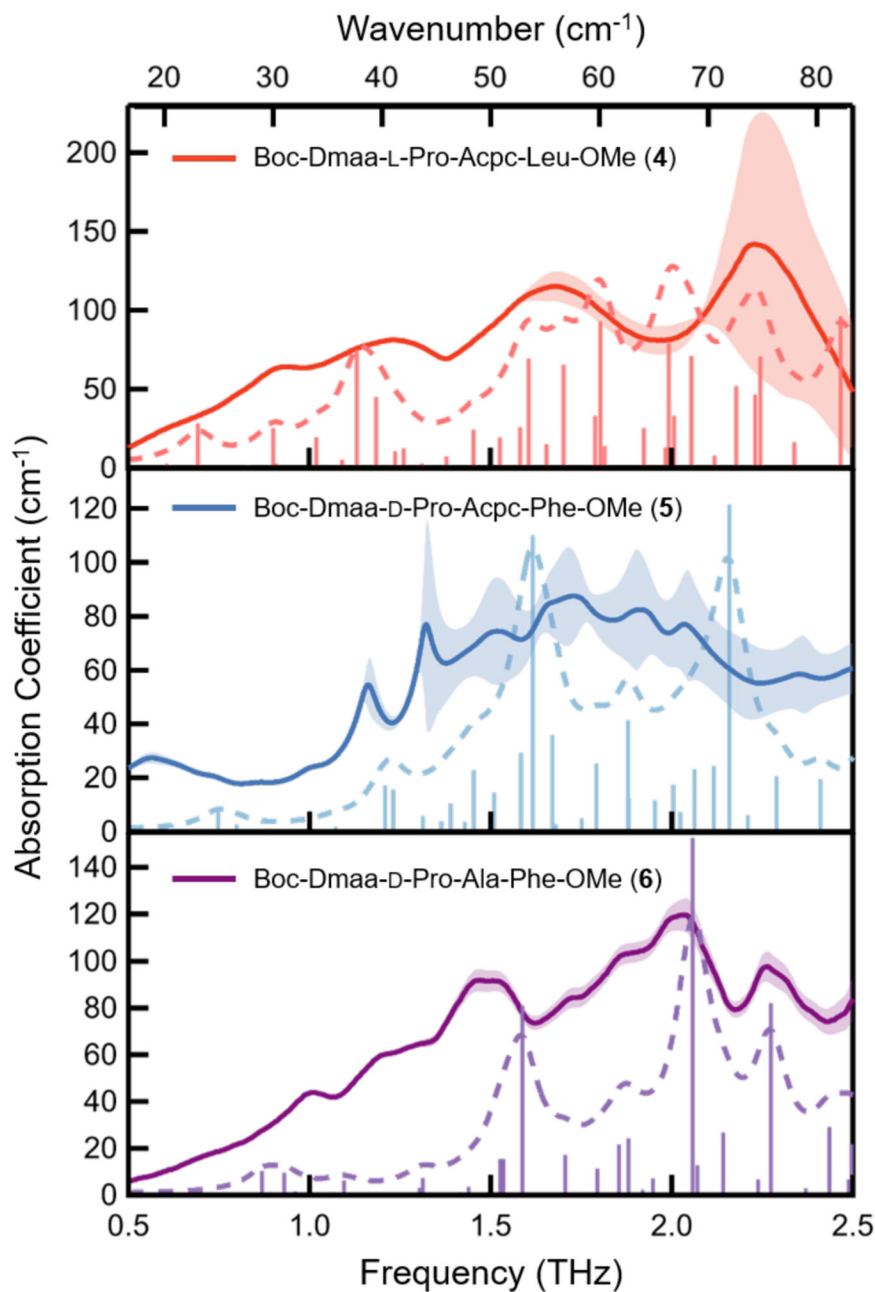


Figure 3. Experimental absorption spectra (solid line) and corresponding calculated DFT spectra (dashed line) for peptides **4** (red), **5** (blue), and **6** (purple). The frequency axis of the DFT calculations are scaled by 0.88 and the single-point IR intensities (shown as stick spectra) are convoluted with Lorentzian functions with a line width of 0.13 THz shown with the dashed lines. Standard deviations for the experimental data are shown by shading around each spectrum.

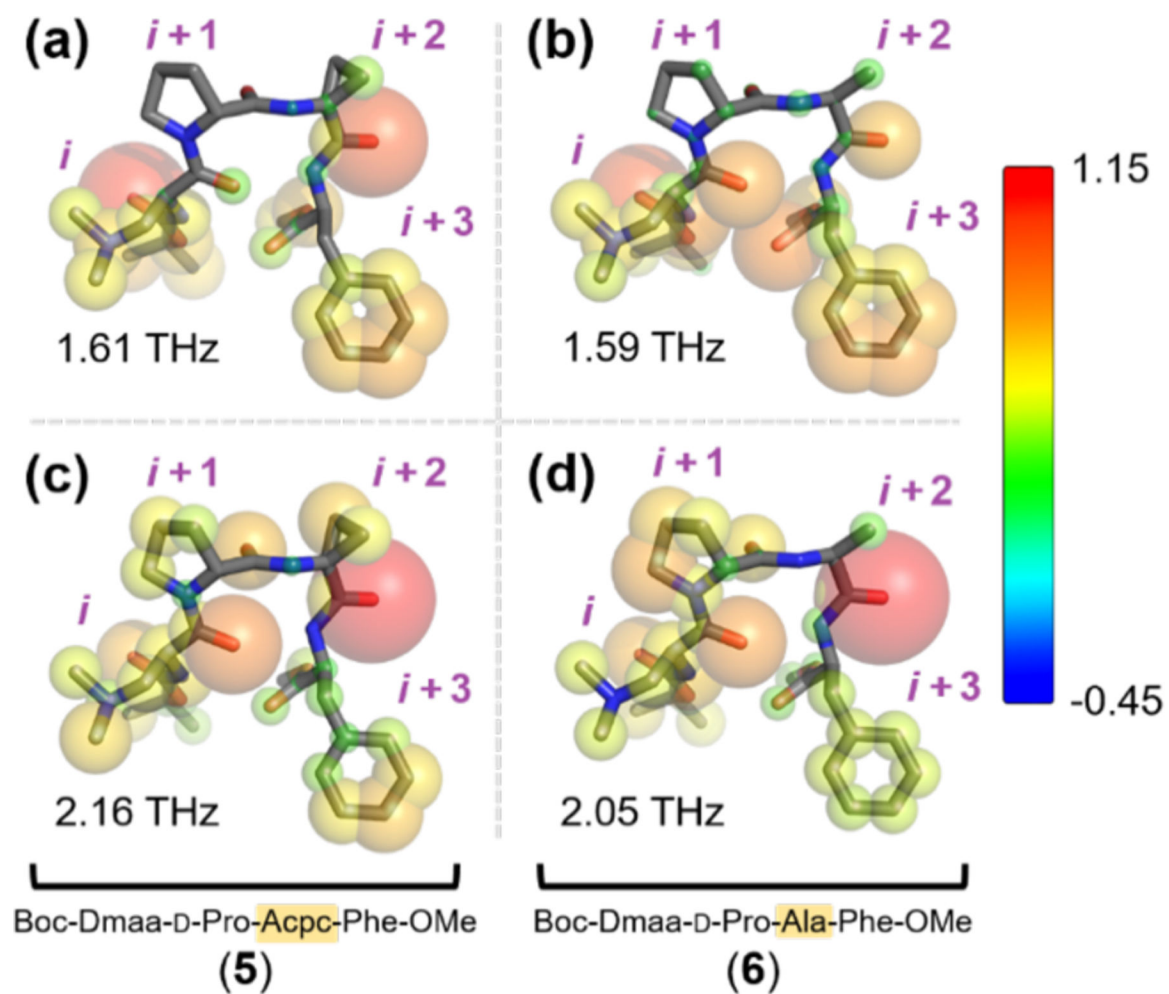


Figure 4.

Heatmaps visualizing the displacement of each atom at the indicated resonance frequency comparing **5** at (a) 1.61 THz and (c) 2.16 THz with **6** at (b) 1.59 THz and (d) 2.05 THz. For clarity, the logarithm of each eigenvector was used in the heatmaps above.